

The production of η -mesons in nucleon-nucleon collisions near threshold

Göran Fäldt¹

Division of Nuclear Physics, Box 535, 751 21 Uppsala, Sweden

Colin Wilkin²

Department of Physics & Astronomy, UCL, London WC1E 6BT, UK

November 13, 2018

Abstract

Data on the total cross sections for the $pp \rightarrow pp\eta$, $pn \rightarrow pn\eta$, and $pn \rightarrow d\eta$ reactions and the $pp \rightarrow pp\eta$ differential cross section near threshold are analysed in a one-meson-exchange model. After including initial and final-state nucleon-nucleon distortion, the magnitude and most of the energy dependence are well reproduced. It is found that the contribution of ρ -exchange is larger than that of π -exchange. With destructive ρ/π interference in the pp case, the model explains quantitatively the $pp \rightarrow pp\eta/pn \rightarrow pn\eta$ cross section ratio and the slope of the $pp \rightarrow pp\eta$ differential cross section. Such an agreement would be destroyed by any significant η -exchange term. The residual energy dependence may be associated with η -nucleon rescattering that has not been taken into account. The $pn \rightarrow pn\eta/pn \rightarrow d\eta$ ratio depends weakly upon the nature of the particle exchanges, being determined primarily by the nucleon-nucleon final state interactions. The proton analysing power is predicted to remain small in the low energy region.

PACS: 25.40.Ve, 13.75.Cs, 25.10.+s

Corresponding author:
Colin Wilkin,
Physics & Astronomy Dept.,
UCL, Gower St.,
London WC1E 6BT, U.K.

¹Electronic address: faldt@tsl.uu.se

²Electronic address: cw@hep.ucl.ac.uk

1 Introduction

The experimental database on η production in nucleon-nucleon scattering has expanded significantly in recent years. The excitation function of the $pp \rightarrow pp\eta$ total cross section shows such a rapid rise with excess energy Q [1, 2, 3, 4], that the major error is often associated with the determination of Q rather than of the cross section itself. Equally striking is the large cross section found for quasi-free η production on a deuterium target [1]; under conditions of well-controlled kinematics the $pn \rightarrow pn\eta/pp \rightarrow pp\eta$ ratio is found to be over 6 near threshold [5, 6]. The CELSIUS group has also measured the $pn \rightarrow d\eta$ total cross section at well-defined c.m. energies [6, 7] and found the first evidence of $N^*(1535)$ dominance from the energy dependence. More tantalisingly, they showed that at very small Q there appears to be a threshold enhancement [8] which, though not as spectacular as that found in the analysis [9] of early Saclay data, nevertheless indicates a strong η -deuteron scattering length.

The only measurement of the angular distribution of η -mesons near threshold suggests that d -waves cannot be neglected in the η -(NN) system for $Q \approx 30$ MeV [10]. It is here important to note that the differential cross section has the opposite curvature to that of $\pi^-p \rightarrow \eta n$ and we will argue that this helps to identify the reaction mechanism. In view of these new data, as well as the experimental advances in $\pi^-p \rightarrow \eta n$ and especially $\gamma p \rightarrow \eta p$, we believe that it is useful to revisit the phenomenological analysis of these reactions.

In the usual theoretical approach, the $N^*(1535)$ (or other) isobar is excited in nucleon-nucleon collisions through the exchange of a single meson X [11, 12, 13, 14, 15, 16, 17]. The $N^*(1535)$ has a large branching ratio into ηN so that, after its decay, one is left with an η plus two nucleons in the final state. Though the philosophies are generally rather similar, the theoretical calculations differ in their details as to which exchanges are relevant, the structure of their coupling, and the importance of the associated form factors. Different techniques have been used in order to include the effects of the initial nucleon-nucleon distortion and the final-

state interactions. The neutron-proton final-state interaction can also produce a deuteron in the exit channel and, as we shall see, the ratio of the $pn \rightarrow d\eta$ and $pn \rightarrow np\eta$ cross sections is determined primarily by low-energy neutron-proton dynamics with a weaker dependence upon the production mechanism [18].

It is generally agreed that in the near-threshold region, $Q \leq 40$ MeV, the energy variation of the total cross section for the $NN\eta$ channel is fixed mainly by the Q^2 factor coming from phase space, modified by the nucleon-nucleon final-state interaction. It is known, however, that η rescattering does produce threshold enhancements in the $pd \rightarrow {}^3\text{He}\eta$ [19] and $dd \rightarrow {}^4\text{He}\eta$ [20] reactions and it is likely that the residual energy dependence in the $pp \rightarrow pp\eta$ excitation function could be due to such an effect. The energy dependence coming from the input single-nucleon production amplitudes is rather modest over a small range in Q .

The relativistic Born amplitudes for single-meson exchange are first evaluated at threshold by neglecting all distortions. To include the effects of the final-state interactions it is, however, necessary to construct a potential from the amplitudes and this is most easily done in configuration space. The energy and angular dependence coming from $\pi^-p \rightarrow \eta n$ and the other elementary amplitudes can then be introduced in a perturbation approach.

The kinematics of the processes are outlined in Section 2. As exchanged particles, we consider the π , η , ρ , and ω . The forms of their coupling to the nucleon are given in Section 3, together with the coupling constants used in this work, though it must be stressed that the uncertainty in the ηNN value is very large. Values for the $XN \rightarrow \eta N$ amplitudes are also discussed in this section. There are, of course, measurements of the pion-induced cross section and the η -nucleon elastic cross section can be deduced from this inside a unitary model. To obtain the necessary vector meson information, we interpret photoproduction data within the framework of the vector meson dominance approach.

The formulae for the bare meson exchange $NN \rightarrow NN\eta$ and $pn \rightarrow d\eta$ amplitudes are derived in Section 4; the energy and angular dependence coming from the $XN \rightarrow \eta N$ amplitudes are there introduced.

Section 5 is devoted to the evaluation of the final state interactions in the pp and np systems. It is found that the enhancement factor varies very fast with excitation energy, and also depends upon isospin in the NN channel as well as on the mass of the exchanged meson. In contrast, the distortion of the initial nucleon-nucleon wave is slowly varying and we try to include its effects simply by using the imaginary part of the relevant phase shift. The η -nucleon final-state interaction is not taken into account, since it would require a consistent three-body treatment in order to include this simultaneously with the nucleon-nucleon interaction. There is, moreover, as yet no credible η -nucleon potential from which to calculate the wave function at short distances. The two-body $pn \rightarrow d\eta$ amplitude is discussed in Section 6.

As shown in Section 7, ρ -exchange is more important than π -exchange, with the ω giving only minor modifications. Taking the ρ/π interference to be destructive in the proton-proton case, these three exchanges reproduce well the measured 6.5 : 1 $pn : pp$ ratio. Since pure η exchange would lead to a ratio of below 1, the results yield an upper bound on the poorly determined η -nucleon coupling constant. With standard parameters, the model reproduces well the magnitude and most of the energy dependence observed in the total cross. There is an indication that the model underpredicts the $pp \rightarrow pp\eta$ data at low Q and the same is true for the two-body $pn \rightarrow d\eta$ results. This is probably due to the neglect of η rescattering. On the other hand, the reasonable agreement found for the $\sigma(pn \rightarrow pn\eta)/\sigma(pn \rightarrow d\eta)$ cross section ratio is mainly a reflection of the np final state interaction.

The dominance of the ρ and the destructive effect of the π explains also the shape of the η angular distribution in $pp \rightarrow pp\eta$, that is larger at 90° than in the forward direction [10]. There are still insufficient input data to give definitive predictions for the proton analysing power, but the indications are that this should be rather small in the near-threshold region. Our conclusions are given in Section 8.

2 Kinematics

We wish to describe the $pp \rightarrow pp\eta$, $pn \rightarrow pn\eta$ and $pn \rightarrow d\eta$ reactions in the near-threshold domain. The energies of the incident nucleons in the c.m. system are denoted by E and their momenta $\pm\mathbf{p}$. At threshold they are related to the nucleon and η masses, M and μ , by

$$\begin{aligned} E &= M + \frac{1}{2}\mu \\ p &= \sqrt{\mu M + \frac{1}{4}\mu^2}. \end{aligned} \quad (2.1)$$

The excess energy Q is fixed by the total c.m. energy as $W = 2E = 2M + m_\eta + Q$, where we shall neglect the neutron-proton mass difference except in the determination of Q from the beam energy. In the case of the two-body $pn \rightarrow d\eta$ reaction, the $2M$ is replaced by the deuteron mass, M_d . Reduced masses in the final state are defined by

$$\mu_\eta = \frac{\mu}{1 + \mu/2M} \quad \mu_{12} = M/2. \quad (2.2)$$

As an alternative to Q , experimentalists often quote the value of the maximum η momentum, p_η , in units of the η mass;

$$\eta = \frac{p_\eta^{\max}}{\mu} = \sqrt{\frac{2\mu_\eta Q}{\mu^2}}. \quad (2.3)$$

If the matrix element \mathcal{M} were constant at its threshold value, the only energy dependence in the unpolarised total cross section would come from the Q^2 factor arising from phase space. Thus, for the reaction $pp \rightarrow pp\eta$,

$$\sigma(pp \rightarrow pp\eta) = \frac{1}{64\pi^2 p W} \frac{(\mu_\eta \mu_{12})^{3/2}}{8M^2 \mu} Q^2 \left[\frac{1}{4} \sum |\mathcal{M}|^2 \right], \quad (2.4)$$

where the summation is over the initial and final spin projections. This expression incorporates a factor of one-half coming from the identity of the final-state protons. Such a factor is absent from the corresponding $pn \rightarrow pn\eta$ formula.

Finally, we also need the cross section for $pn \rightarrow d\eta$, which is

$$\sigma(pn \rightarrow d\eta) = \frac{1}{16\pi W^2} \frac{p_\eta}{p} \left[\frac{1}{4} \sum |\mathcal{M}|^2 \right]. \quad (2.5)$$

As we shall see later, the strong nucleon-nucleon final state interaction will lead to a major modification in the Q^2 behaviour such that it will no longer be permissible to factorise the dynamics from the phase space, as has been done in Eq. (2.4).

3 Input Amplitudes and Vertices

The basic inputs required for the evaluation of our Feynman diagrams are vertex functions and η -production amplitudes \mathcal{M} , which are the matrix elements of $i\mathcal{L}_{\text{int}} = -i\mathcal{H}_{\text{int}}$. We list below their general forms as well as the corresponding approximations used in the evaluation of the near-threshold amplitudes.

3.1 Pseudoscalar meson-nucleon vertex

The standard πNN coupling in terms of four-component spinors $u(p)$ is

$$\mathcal{M}_{\pi NN} = -\frac{f_\pi}{m_\pi} \bar{u}(\mathbf{p}') \gamma_5 (\not{p}' - \not{p}) \boldsymbol{\tau} \cdot \boldsymbol{\phi}_\pi u(\mathbf{p}), \quad (3.6)$$

where we take the pion-nucleon coupling

$$G_\pi = \frac{2Mf_\pi}{m_\pi} \quad (3.7)$$

to have the numerical value $G_\pi^2/4\pi = 13.6$ [21]. Since we are specialising to near-threshold reactions, it is sufficient in our applications to put $\mathbf{p}' = \mathbf{0}$ and $E' = M$ in the final state.

It is important to take into account the off-shell extrapolation in the vertex function and for this we introduce a monopole form factor

$$F_\pi(q^2) = \frac{\Lambda_\pi^2 - m_\pi^2}{\Lambda_\pi^2 - q^2}, \quad (3.8)$$

where q^2 is the square of the pion four-momentum. We take the value $\Lambda_\pi = 1.72$ GeV/c, as recommended in [21].

The size of the η -nucleon coupling constant is extremely uncertain, with values of $G_\eta^2/4\pi$ between 0 and 7 being quoted in the literature (see *e.g.* [22]). A value of 0.4 has been deduced from fits to photoproduction [23]. However, even with a value as small as that, it is claimed that η -exchange would strongly influence η production in nucleon-nucleon collisions [16]. Since pure η -exchange gives a completely wrong prediction for the ratio of the relative production in the pp and pn cases, these data will provide evidence for some upper limit for $G_\eta^2/4\pi$ within the framework of the meson-exchange model for η production.

The range parameter in the η form factor will be taken, as in the Bonn meson-exchange potential [24], to have the value $\Lambda_\eta = 1.5$ GeV.

3.2 Vector-meson-nucleon vertex

The generic form of the couplings of vector mesons to the nucleon is (see *e.g.* [25])

$$\begin{aligned}\mathcal{M}_{VNN} &= -ig_V \bar{u}(\mathbf{p}') \left[\not{\epsilon} + \frac{\kappa_V}{4M} (\not{\epsilon} \not{k} - \not{k} \not{\epsilon}) \right] u(\mathbf{p}), \\ &= -ig_V \epsilon \cdot V,\end{aligned}\tag{3.9}$$

where $k = p' - p$ is the four-momentum of the vector meson and $\epsilon = \epsilon(k)$ its polarisation four-vector.

The numerical values of the ρ and ω coupling constants are, according to [21],

$$\begin{aligned}g_\rho &= 3.25, & \kappa_\rho &= 6.1, \\ g_\omega &= 15.9, & \kappa_\omega &= 0.0.\end{aligned}\tag{3.10}$$

As in the Bonn potential [24, 21] we shall use the monopole form factors of Eq. (3.8) with numerical values $\Lambda_\rho = 1.4$ GeV/c and $\Lambda_\omega = 1.5$ GeV/c.

To take account of the $I = 1$ nature of the ρ meson, the vertex function in Eq. (3.9) must be multiplied by an isospin factor $\boldsymbol{\tau} \cdot \boldsymbol{\phi}_\rho$ in analogy to the pion-nucleon vertex.

3.3 Pseudoscalar meson-induced η production

In the absence of polarisation data, the spin-non-flip $\pi N \rightarrow \eta N$ amplitude is sufficient to describe the bulk of the experimental data near threshold. In the two-component reduction this has the structure

$$\mathcal{M}(\pi N \rightarrow \eta N) = \bar{u}(\mathbf{p}') [-ih_\pi] \boldsymbol{\tau} \cdot \boldsymbol{\phi}_\pi u(\mathbf{p}),\tag{3.11}$$

where h_π may depend upon the production angle θ . For neutral pions the c.m. differential cross section becomes

$$\frac{d\sigma}{d\Omega}(\pi^0 N \rightarrow \eta N) = \frac{p_\eta}{p} \frac{1}{16\pi^2} |h_\pi|^2 \left(1 + \frac{\mu^2 - m_\pi^2}{4M(M + \mu)} \right) \frac{1}{(1 + \mu/M)^2},\tag{3.12}$$

whereas for charged pions the cross section is a factor of two bigger.

Until the large Crystal Ball data set is fully analysed [26], the available results on the $\pi^-p \rightarrow \eta n$ differential cross section are generally far less systematic than those for photoproduction. Parameterising the differential cross section as

$$\frac{d\sigma}{d\Omega} = \frac{p_\eta}{p} [b_0 P_0(\cos\theta) + b_1 P_1(\cos\theta) + b_2 P_2(\cos\theta)] , \quad (3.13)$$

the threshold value was determined many years ago as $4\pi b_0 = (9.1 \pm 0.8)$ mb [27]. This is a little higher than the first Crystal Ball measurement at 720 MeV/c, that gives $4\pi b_0 = (7.4 \pm 0.3)$ mb [28]. This group has also a preliminary determination of the *shape* of the differential cross section at (716 ± 16) MeV/c, which leads to $b_1/b_0 = -0.042$ and $b_2/b_0 = 0.137$ [29]. Assuming an energy dependence of the total cross section similar that for photoproduction shown in Eq. (3.26), we fix the $\pi^0 p \rightarrow \eta p$ amplitude squared to be

$$|h_\pi|^2 = [(128 - 303\eta^2)P_0(\cos\theta) + 23\eta P_1(\cos\theta) + 342\eta^2 P_2(\cos\theta)] \text{ mb/sr} . \quad (3.14)$$

There are as yet no measurements of the proton analysing power near threshold, but the smallness of the P_1 coefficient in Eq. (3.14) suggests the angular dependence arises primarily from the interference of a small spin-non-flip d -wave with the dominant s -wave. This could for example be due to the tail of the D_{13} resonance. We therefore neglect the P_1 term and take

$$h_\pi = h_\pi^0 + \frac{1}{2}h_\pi^2 \left(3(\hat{\mathbf{p}}_\eta \cdot \hat{\mathbf{k}})^2 - 1 \right) , \quad (3.15)$$

where

$$|h_\pi^0|^2 = (128 - 303\eta^2) \text{ mb/sr} , \quad \text{Re}[h_\pi^2/h_\pi^0] = 1.3\eta^2 . \quad (3.16)$$

Multiresonance fits to projections of $\pi^-p \rightarrow \eta n$ and $\pi^-p \rightarrow \pi^-p/\pi^0 n$ data onto the S_{11} channel allow one to estimate the η -nucleon elastic scattering amplitude. Although the results, especially on the real part, are rather sensitive to the assumptions made [30, 31], a typical value of the scattering length is $a_{\eta N} = (0.83 + 0.27i)$ fm. The elastic η -nucleon scattering amplitude corresponding to Eq. (3.11) is

$$h_\eta = -4\pi \left(1 + \frac{\mu}{M} \right) a_{\eta N} . \quad (3.17)$$

The exchanged mesons are far from the mass shell in our model. We assume that the effects of this can be taken into account by multiplying the pion-exchange amplitude by the monopole form factor $F_\pi(q^2)$ of Eq. (3.8), and similarly for η exchange.

3.4 Vector-meson-induced η production

Although nothing is known directly about η production by vector mesons, one can use the vector-meson dominance model (VMD) to relate photon- and vector-meson-induced reactions [33].

The isovector component of the photon couples to the ρ field and the isoscalar part to the ω , though such an identification is only valid for transversely polarised vector mesons. Neglecting higher mass vector mesons, the photoproduction amplitude may be written in terms of off-shell strong-interaction amplitudes as

$$\mathcal{M}(\gamma p \rightarrow \eta p) = \frac{e}{f_\rho} \mathcal{M}_\perp(\rho_0 p \rightarrow \eta p) + \frac{e}{f_\omega} \mathcal{M}_\perp(\omega p \rightarrow \eta p), \quad (3.18)$$

with an analogous relation for neutron targets.

Since universality is broken in the VMD model, we choose as effective ρ -meson coupling constant the geometric mean of the two values derived by Benayoun *et al.* [34],

$$\frac{f_\rho^2}{4\pi} = 2.4. \quad (3.19)$$

This number is in reasonable agreement with those extracted from ρ -photoproduction [35].

The value of the ω coupling constant is less certain. Here we have chosen to scale it to the ρ coupling according to the $\Gamma(\rho \rightarrow e^+e^-)$ and $\Gamma(\omega \rightarrow e^+e^-)$ decay widths, giving

$$\frac{f_\omega^2}{4\pi} = 27. \quad (3.20)$$

Data on the photoproduction of η 's on deuterium show that near threshold $\sigma(\gamma n \rightarrow \eta n)/\sigma(\gamma p \rightarrow \eta p) = 0.66 \pm 0.03$, where some attempt has been made to include the systematic error arising from the use a deuteron target [32]. The low cross section found for the coherent $\gamma d \rightarrow \eta d$ reaction [32] implies that isovector

photons dominate the production, so that the amplitude ratio is negative:

$$r = -\frac{\mathcal{M}(\gamma n \rightarrow \eta n)}{\mathcal{M}(\gamma p \rightarrow \eta p)} = 0.81 \pm 0.02. \quad (3.21)$$

The vector-meson-induced amplitudes thus become

$$\begin{aligned} \mathcal{M}_\perp(\rho_0 p \rightarrow \eta p) &= \frac{f_\rho}{e} \left(\frac{1+r}{2} \right) \mathcal{M}(\gamma p \rightarrow \eta p), \\ \mathcal{M}_\perp(\omega p \rightarrow \eta p) &= \frac{f_\omega}{e} \left(\frac{1-r}{2} \right) \mathcal{M}(\gamma p \rightarrow \eta p). \end{aligned} \quad (3.22)$$

The threshold photoproduction amplitude is proportional to $\boldsymbol{\sigma} \cdot \boldsymbol{\epsilon}_\gamma$. The gauge-invariant photoproduction amplitude that reduces to the correct threshold S-wave limit is

$$\mathcal{M}_\gamma = R_\gamma \frac{1}{2} \bar{u}(\mathbf{p}') \gamma_5 (\not{\epsilon} \not{k} - \not{k} \not{\epsilon}) u(\mathbf{p}) \longrightarrow 8\pi W E_{0+} \eta^\dagger \boldsymbol{\sigma} \cdot \boldsymbol{\epsilon} \zeta, \quad (3.23)$$

where

$$E_{0+} = \frac{1}{8\pi W} \sqrt{(E+M)(E'+M)} (W-M) R_\gamma, \quad (3.24)$$

with k the photon momentum four-vector and W the c.m. energy.

Assuming, as for the pion-induced reaction, that there is also a contribution from the D_{13} resonance as well as the S_{11} at low energies, the more general reduction is

$$\mathcal{M}_\gamma \longrightarrow 8\pi W \eta^\dagger \left(E_{0+} \boldsymbol{\sigma} \cdot \boldsymbol{\epsilon} + \frac{1}{2} E_{2-} [3\boldsymbol{\sigma} \cdot \hat{\mathbf{q}} \hat{\mathbf{q}} \cdot \boldsymbol{\epsilon} - \boldsymbol{\sigma} \cdot \boldsymbol{\epsilon}] \right) \zeta, \quad (3.25)$$

Taking the d -wave to first order, the unpolarised photoproduction differential cross section is related to these multipoles through

$$\frac{d\sigma}{d\Omega}(\gamma p \rightarrow \eta p) = \frac{k_\eta}{k} |E_{0+}|^2 \left(1 + \text{Re}(E_{2-}/E_{0+}) [3(\hat{\mathbf{q}} \cdot \hat{\mathbf{k}})^2 - 1] \right). \quad (3.26)$$

The near-threshold $\gamma p \rightarrow \eta p$ differential cross section [32] can be parameterised [36]

$$\frac{d\sigma}{d\Omega} = \frac{k_\eta}{k} [(4.59 - 10.9\eta^2) P_0(\cos\theta) - 0.291\eta P_1(\cos\theta) - 3.21\eta^2 P_2(\cos\theta)] \mu\text{b/sr}. \quad (3.27)$$

Neglecting the P_1 term, which must arise from an interference with a small p -wave component, we deduce that

$$|E_{0+}|^2 = (4.59 - 10.9\eta^2) \mu\text{b/sr}, \quad \text{Re}(E_{2-}/E_{0+}) = -0.70\eta^2. \quad (3.28)$$

At threshold $|E_{0+}| = 0.0214 \text{ fm}$ and hence $|R_\gamma| = 0.146 \text{ fm}^2$. The energy variation of E_{0+} is mainly a reflection of the dominance of the $N^*(1535)$ resonance near the η threshold.

In the same approximation, the proton analysing power is [36]

$$A_y = -3 \text{Im}(E_{2-}/E_{0+}) \sin\theta \cos\theta. \quad (3.29)$$

A_y remains small for photon energies below 850 MeV [37], with evidence for both sp and sd interference. This gives

$$\text{Im}(E_{2-}/E_{0+}) = (-3 \pm 0.5)\eta^2 + (16 \pm 4)\eta^4. \quad (3.30)$$

We now make the *ad hoc* assumption that all three polarisation states have the same strength in the vector-meson-induced reaction. The amplitude is then proportional to $\boldsymbol{\sigma} \cdot \boldsymbol{\epsilon}_V$, with the proportionality constant being determined by the vector-meson-dominance model. The relativistic form which has this limit is

$$\begin{aligned} \mathcal{M}(Vp \rightarrow \eta p) &= R_V \bar{u}(\mathbf{p}') \left[\frac{1}{2} \gamma_5 (\not{\epsilon} \not{k} - \not{k} \not{\epsilon}) + m_V \gamma_5 \not{\epsilon} \right] u(\mathbf{p}) \\ &= \sqrt{(E+M)(E'+M)} (W-M+m_V) R_V \eta^\dagger \boldsymbol{\sigma} \cdot \boldsymbol{\epsilon} \zeta. \end{aligned} \quad (3.31)$$

The scale factors R_V are determined from the VMD model, Eqs. (3.22), evaluated at the η threshold $W = M + \mu$:

$$R_\rho = R_\gamma \frac{f_\rho}{e} \left(\frac{1+r}{2} \right) \left[\frac{\mu}{\mu+m_\rho} \right], \quad R_\omega = R_\gamma \frac{f_\omega}{e} \left(\frac{1-r}{2} \right) \left[\frac{\mu}{\mu+m_\omega} \right]. \quad (3.32)$$

From the value of R_γ , we deduce that $|R_\rho| = 0.916 \text{ fm}^2$ and $|R_\omega| = 0.310 \text{ fm}^2$ at threshold.

As before, we attempt to describe the off-shell extrapolation through a form factor. Since we are starting from data with zero-mass photons, the correct form factor at the ρ -induced photoproduction vertex is

$$\tilde{F}_\rho(q^2) = F_\rho(q^2)/F_\rho(0). \quad (3.33)$$

We take for $F_\rho(q^2)$ the monopole form factor of Eq. (3.8). This is not in contradiction with the off-shell behaviour of the η -photoproduction amplitude measured *via* electron scattering at modest q^2 [38].

3.5 Deuteron vertex

Both nucleons are close to their mass shells at the deuteron vertex, so that each pole gives a contribution after integration over the internal energy variable. The deuteron vertex matrix element corresponding to the deuteron S- and D-state wave functions $\phi_S(r)$ and $\phi_D(r)$ is

$$\begin{aligned}
& iS_F^c(k) (-i\Gamma \cdot \epsilon_d^*) iS_F(p_d - k) = \\
& u_c(\mathbf{k}) (2\pi)^{3/2} \eta_c^\dagger \frac{-1}{\sqrt{2}} \left[\boldsymbol{\sigma} \cdot \boldsymbol{\epsilon}_d^\dagger \phi_S(\mathbf{Q}_R) + \left\{ \boldsymbol{\sigma} \cdot \boldsymbol{\epsilon}_d^\dagger - 3\boldsymbol{\sigma} \cdot \hat{\mathbf{Q}}_R \boldsymbol{\epsilon}_d^\dagger \cdot \hat{\mathbf{Q}}_R \right\} \phi_D(\mathbf{Q}_R) \right] \zeta \bar{u}(\mathbf{p}_d - \mathbf{k}) \\
& \quad \times \frac{\sqrt{2M_d}}{2M} (2\pi) \{ \delta(k^0 - E_n) + \delta(p_d^0 - k^0 - E_p) \}. \tag{3.34}
\end{aligned}$$

E_n and E_p are the nucleon on-shell energies so that, *e.g.* $E_n = \sqrt{\mathbf{k}^2 + M^2}$, and \mathbf{Q}_R is the proton-neutron relative momentum.

4 Amplitude for $pp \rightarrow pp\eta$

We describe the reaction $pp \rightarrow pp\eta$ in terms of Feynman diagrams, the prototype of which is displayed in Fig. 1, considering the four exchanges, ρ , ω , π , and η . The matrix elements are evaluated at threshold, where the momenta in the final state vanish and the values of the corresponding incident proton energies and momenta are given in Eq. (2.1). We first study neutral-particle exchanges; the necessary isospin factors will be derived at the end of the section.

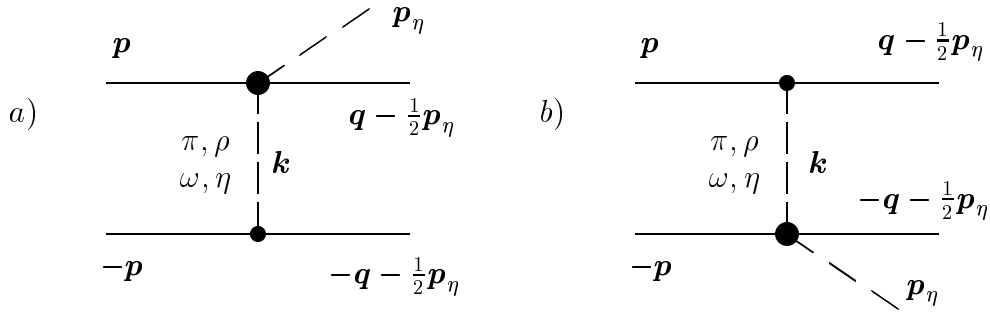


Figure 1: Meson exchange diagrams for $pp \rightarrow pp\eta$. Diagrams $c)$ and $d)$ are obtained from $a)$ and $b)$ by interchanging the final state nucleons.

4.1 Vector-exchange diagrams

The propagator for vector meson exchange is

$$iD_{\mu\nu}(k, m) = \frac{i(-g_{\mu\nu} + k_{\mu}k_{\nu})}{k^2 - m_V^2}. \quad (4.35)$$

When the vector meson four-momentum k_{μ} is contracted into the VNN vertex, it vanishes identically. We thus obtain for ρ^0 exchange in diagram a

$$\mathcal{M}_a(pp \rightarrow pp\eta) = \mathcal{M}_{\mu}(p \rightarrow p\rho^0) \frac{-i}{k^2 - m_{\rho}^2} \mathcal{M}^{\mu}(\rho^0 p \rightarrow \eta p). \quad (4.36)$$

Using the expressions for the matrix elements of the vertex ρpp and amplitude $\rho p \rightarrow \eta p$, given in Eqs. (3.9) and (3.30), leads to the threshold expression

$$\mathcal{M}_a(pp \rightarrow pp\eta) = 4M \frac{g_{\rho} R_{\rho}}{M_{\mu} + m_{\rho}^2} \left[F_{\rho}^2(-M_{\mu}) / F_{\rho}(0) \right] \mathcal{K}_a, \quad (4.37)$$

with

$$\mathcal{K}_a = a [\eta_3^\dagger \boldsymbol{\sigma} \cdot \mathbf{p} \zeta_1] [\eta_4^\dagger \zeta_2] - ib [\eta_3^\dagger \boldsymbol{\sigma} \zeta_1] \cdot [\eta_4^\dagger \mathbf{p} \times \boldsymbol{\sigma} \zeta_2]. \quad (4.38)$$

The parameters a and b are given by

$$\begin{aligned} a &= (M - m_\rho) \left(1 - \frac{\mu \kappa_\rho}{4M}\right), \\ b &= \frac{1}{2} (m_\rho + \mu) (1 + \kappa_\rho). \end{aligned} \quad (4.39)$$

The momentum of the intermediate vector meson is $\mathbf{k} = -\mathbf{p}$ and the form factor is evaluated at mass squared $k^2 = -M\mu$.

We can similarly write down the expression for diagram b , where the two vertices are interchanged:

$$\mathcal{K}_b = -a [\eta_3^\dagger \zeta_1] [\eta_4^\dagger \boldsymbol{\sigma} \cdot \mathbf{p} \zeta_2] + ib [\eta_3^\dagger \mathbf{p} \times \boldsymbol{\sigma} \zeta_1] \cdot [\eta_4^\dagger \boldsymbol{\sigma} \zeta_2], \quad (4.40)$$

with $\mathbf{k} = +\mathbf{p}$.

It is easy to interpret the b -terms if we explicitly write the sum over the polarisation states of the ρ meson. Thus, in Eq. (4.38), this gives

$$[\eta_3^\dagger \boldsymbol{\sigma} \zeta_1] [\eta_4^\dagger \mathbf{p} \times \boldsymbol{\sigma} \zeta_2] = \sum [\eta_3^\dagger \boldsymbol{\sigma} \cdot \boldsymbol{\epsilon}_\rho \zeta_1] [\eta_4^\dagger \boldsymbol{\epsilon}_\rho \cdot (\mathbf{p} \times \boldsymbol{\sigma}) \zeta_2] \quad (4.41)$$

Here we recognise the vertex for the ρNN coupling as $\boldsymbol{\epsilon}_\rho \cdot (\mathbf{k} \times \boldsymbol{\sigma})$ and that for ρ -induced η production as $\boldsymbol{\sigma} \cdot \boldsymbol{\epsilon}_\rho$. The small a -term arises from the part of the ρNN coupling that contains the vertex factor $\boldsymbol{\epsilon}_\rho \cdot \mathbf{k}$.

At threshold the initial total spin of the pp system is $S = 1$ with $S = 0$ in the final state and we shall let $\boldsymbol{\epsilon}$ denote the spin vector of the spin-one pp state and $\boldsymbol{\eta}$ the spin-zero state vector. The contribution of diagrams a and b is the same as that for the crossed diagrams c and d :

$$\mathcal{K}_a + \mathcal{K}_b = \mathcal{K}_c + \mathcal{K}_d = -2(2b - a) \mathbf{p} \cdot \boldsymbol{\epsilon}_i \boldsymbol{\eta}_f. \quad (4.42)$$

From Eq. (4.37) and (4.42), the total ρ^0 contribution becomes

$$\mathcal{M}_\rho(pp \rightarrow pp\eta) = (\mathcal{A}_\rho - 2\mathcal{B}_\rho) \mathbf{p} \cdot \boldsymbol{\epsilon}_i \boldsymbol{\eta}_f, \quad (4.43)$$

where

$$\begin{aligned}\mathcal{A}_\rho &= 16M \frac{g_\rho R_\rho}{M\mu + m_\rho^2} \left[F_\rho^2(-M\mu)/F_\rho(0) \right] a, \\ \mathcal{B}_\rho &= 16M \frac{g_\rho R_\rho}{M\mu + m_\rho^2} \left[F_\rho^2(-M\mu)/F_\rho(0) \right] b.\end{aligned}\quad (4.44)$$

With the values of the parameters given in section 3, it can be seen that the \mathcal{A} -term is of no numerical importance for ρ exchange.

When the d -waves are included in the dominant b -term, the amplitude of Eq. (4.43) is modified slightly to read

$$\mathcal{M}_\rho(pp \rightarrow pp\eta) = (\mathcal{A}_\rho - 2\mathcal{B}_\rho) \left[\mathbf{p} \cdot \boldsymbol{\epsilon}_i + \frac{1}{2}(E_{2-}/E_{0+})(3\mathbf{p} \cdot \hat{\mathbf{q}} \hat{\mathbf{q}} \cdot \boldsymbol{\epsilon}_i - \mathbf{p} \cdot \boldsymbol{\epsilon}_i) \right] \eta_f. \quad (4.45)$$

To first order in E_{2-}/E_{0+} , this gives exactly the same form as in the $\gamma p \rightarrow \eta p$ cross section of Eq. (3.26).

The amplitudes for ω are completely analogous to those for ρ exchange, so that at threshold

$$\mathcal{M}_\omega(pp \rightarrow pp\eta) = (\mathcal{A}_\omega - 2\mathcal{B}_\omega) \mathbf{p} \cdot \boldsymbol{\epsilon}_i \eta_f, \quad (4.46)$$

where the amplitudes are as defined in Eq. (4.44) and the parameters in Eq. (4.39).

4.2 Pseudoscalar-exchange diagrams

The four diagrams with π^0 exchange are labelled as in Fig. 1. The contribution from diagram a is

$$\mathcal{M}_a(pp \rightarrow pp\eta) = \mathcal{M}(p \rightarrow p\pi^0) \frac{i}{k^2 - m_\pi^2} \mathcal{M}(\pi^0 p \rightarrow \eta p). \quad (4.47)$$

Inserting the forms for the πpp vertex and η -production amplitude, given by Eq. (3.6) and (3.11), into Eq. (4.47) yields

$$\mathcal{M}_a(pp \rightarrow pp\eta) = 2MG_\pi h_\pi \frac{1}{M\mu + m_\pi^2} \left[F_\pi^2(-M\mu) \right] \mathcal{K}_a, \quad (4.48)$$

where

$$\mathcal{K}_a = [\eta_3^\dagger \zeta_1] [\eta_4^\dagger \boldsymbol{\sigma} \cdot \mathbf{p} \zeta_2]. \quad (4.49)$$

Using the same techniques as for ρ exchange, the sum of the amplitudes for diagrams c and d is the same as that for a and b :

$$\mathcal{K}_a + \mathcal{K}_b = \mathcal{K}_c + \mathcal{K}_d = 2 \mathbf{p} \cdot \boldsymbol{\epsilon}_i \eta_f . \quad (4.50)$$

The final result is then

$$\mathcal{M}_\pi(pp \rightarrow pp\eta) = \mathcal{D}_\pi \mathbf{p} \cdot \boldsymbol{\epsilon}_i \eta_f , \quad (4.51)$$

where

$$\mathcal{D}_\pi = 8MG_\pi h_\pi \frac{1}{M\mu + m_\pi^2} \left[F_\pi^2(-M\mu) \right] . \quad (4.52)$$

With the inclusion of d -waves, the input amplitude h_π has an angular dependence given by Eq. (3.15).

The expressions for the η -exchange amplitudes are algebraically identical to those of pion exchange, with the π index being replaced by an η . Of course, as discussed in Section 2, poor knowledge of the value of the ηNN coupling constant makes the strength of any η contribution extremely uncertain.

4.3 Isospin considerations

The expressions derived for the various amplitudes correspond to neutral-meson exchange for the pp case. The $NN \rightarrow NN\eta$ isospin-one production amplitude is

$$\mathcal{M}_1 = \eta_f^\dagger \mathbf{p} \cdot \boldsymbol{\epsilon}_i [(\mathcal{A}_\rho - 2\mathcal{B}_\rho) + (\mathcal{A}_\omega - 2\mathcal{B}_\omega) + \mathcal{D}_\pi + \mathcal{D}_\eta] \boldsymbol{\chi}_f^\dagger \cdot \boldsymbol{\chi}_i . \quad (4.53)$$

It is straightforward to generalise this to the case of isospin zero [11]:

$$\mathcal{M}_0 = \mathbf{p} \cdot \boldsymbol{\epsilon}_f^\dagger \eta_i [-3(\mathcal{A}_\rho + 2\mathcal{B}_\rho) + (\mathcal{A}_\omega + 2\mathcal{B}_\omega) - 3\mathcal{D}_\pi + \mathcal{D}_\eta] \phi_f^\dagger \phi_i . \quad (4.54)$$

Here $\boldsymbol{\chi}$ and ϕ are isospin-1 and -0 operators and the subscripts refer to the particles exchanged.

The spin-average of the square of the matrix element becomes

$$\frac{1}{4} \sum |\mathcal{M}(pp \rightarrow pp\eta)|^2 = \frac{p^2}{4} |(\mathcal{A}_\rho - 2\mathcal{B}_\rho) + (\mathcal{A}_\omega - 2\mathcal{B}_\omega) + \mathcal{D}_\pi + \mathcal{D}_\eta|^2 \quad (4.55)$$

for the pp case and

$$\begin{aligned} \frac{1}{4} \sum |\mathcal{M}(pn \rightarrow np\eta)|^2 &= \frac{p^2}{16} \left[|-3(\mathcal{A}_\rho + 2\mathcal{B}_\rho) + (\mathcal{A}_\omega + 2\mathcal{B}_\omega) - 3\mathcal{D}_\pi + \mathcal{D}_\eta|^2 \right. \\ &\quad \left. + |(\mathcal{A}_\rho - 2\mathcal{B}_\rho) + (\mathcal{A}_\omega - 2\mathcal{B}_\omega) + \mathcal{D}_\pi + \mathcal{D}_\eta|^2 \right] \quad (4.56) \end{aligned}$$

for pn . Application of the formulae in Section 2 then give the cross sections.

4.4 Kinematics

Since we are only considering cases where the excess energy is low, the transformation between the final ηN and ηNN systems is non-relativistic. Taking the laboratory momentum to be the same in the ηN and ηNN cases, one sees that the c.m. momentum is lower in the single-nucleon than the two-nucleon case:

$$\mathbf{p}_{\eta N} = \left(\frac{1 + \mu/2M}{1 + \mu/M} \right) \mathbf{p}_{\eta NN} . \quad (4.57)$$

5 Initial and Final Nucleon-Nucleon Distortion

Most of the energy dependence observed in the cross sections for the $NN \rightarrow NN\eta$ reactions near threshold can be ascribed to the behaviour of the three-body phase space that has been modified by the very strong nucleon-nucleon final state interaction (fsi). It has been traditional to incorporate the effects of such an fsi by multiplying the predicted cross section by a Watson enhancement factor. This prescription gives a rapid energy variation parameterised in terms of the NN scattering length and effective range [39]. It does, however, give too steep a fall at higher NN relative momenta [40] and does not attempt to provide an overall normalisation factor.

In their analysis of the experimental data, the authors of [10] took the enhancement factor as the ratio of the squares of the interacting NN S -state wave function to the equivalent plane wave. In the absence of a model for the η -production operator, they evaluated the ratio at a fixed radius of $r = 1$ fm, which is close to the maximum of the NN density [41].

To obtain more realistic enhancement factors, we must study further the meson-production operator. In the plane-wave approximation, the dominant ρ -exchange contribution from the diagram of Fig. 1a can be described by a potential

$$V_\rho(\mathbf{r}) \propto (\boldsymbol{\sigma}_1 \times \boldsymbol{\sigma}_2) \cdot \hat{\mathbf{r}} \left(1 + \frac{1}{m_\rho^* r} \right) \frac{e^{-m_\rho^* r}}{m_\rho^* r} . \quad (5.58)$$

In the vicinity of the η threshold, the energy transfer is shared equally by the two nucleons, so that the range of this propagation is determined by the reduced ρ -mass, given by

$$m_\rho^{*2} = m_\rho^2 - \omega^2/4 , \quad (5.59)$$

where ω is the total energy of the η meson.

Taking matrix elements of the potential between interacting nucleon but η plane waves and projecting out the threshold angular momentum transition, we are left with the amplitude

$$\mathcal{M}_\rho^{int} = \mathcal{M}_\rho C_\rho \int_0^\infty \psi_k^{(-)*}(r) Y_1(m_\rho^*, r) j_0(\frac{1}{2}p_\eta r) \psi_p^{(+)}(r) r^2 dr , \quad (5.60)$$

with \mathcal{M}_ρ the appropriate plane wave ρ -exchange amplitude of Eq. (4.53) or (4.54), and where

$$C_\rho = \frac{1}{p} m_\rho^{*2} (m_\rho^{*2} + p^2) \quad (5.61)$$

and

$$Y_1(m_\rho^*, r) = \left(1 + \frac{1}{m_\rho^* r}\right) \frac{e^{-m_\rho^* r}}{m_\rho^* r}. \quad (5.62)$$

The wave function $\psi_k(r)$ describes the S -wave of the final $I = 1, J = 0$ or $I = 0, J = 1$ NN system and $\psi_p(r)$ the incident high energy NN P -waves.

The exchange of other negative parity mesons, (ω, π, η) , leads to a very similar structure, though with different effective masses given by Eq. (5.59).

When monopole form factors of the type given in Eq. (3.8) are introduced at the ρNN and production vertices, the only modification to the formula is to replace the $Y_1(m_\rho^*, r)$ propagator in Eq. (5.62) by

$$\bar{Y}_1(m_\rho^*, r) = \frac{(\Lambda^{*2} + p^2)^2}{(\Lambda^{*2} - m_\rho^{*2})^2} \left[Y_1(m_\rho^*, r) - \frac{1}{2m_\rho^{*2}} \left(\frac{2}{r^2} + \frac{2\Lambda^*}{r} + (\Lambda^{*2} - m_\rho^{*2}) \right) e^{-\Lambda^* r} \right], \quad (5.63)$$

with

$$\Lambda^{*2} = \Lambda^2 - \omega^2/4 \quad (5.64)$$

For $r \ll 1/\Lambda^*$, $\bar{Y}_1(m_\rho^*, r) = O(r)$ and so the form factor reduces a little the sensitivity to the small- r components of the wave function.

In order to investigate purely the effect of the NN fsi near threshold, $\psi_k(r)$ is replaced by the plane wave spherical Bessel function $j_1(pr)$. Near threshold the η plane wave factor $j_0(\frac{1}{2}p_\eta r)$ can be taken to be unity. We then quantify the final state enhancement through the ratio of the amplitudes

$$E_x(k) = \mathcal{M}_x^{\text{int}} / \mathcal{M}_x^{\text{pw}} \quad (5.65)$$

calculated from Eq. (5.60) with interacting and plane NN final-state waves.

The enhancement factors $|E_x|^2$ are shown in Fig. 2 for both $I = 0$ and $I = 1$ NN states in the case of ρ -exchange. It can be seen that Coulomb effects are significant for pp final states with $k \leq 0.2 \text{ fm}^{-1}$. For π -exchange the energy dependence is almost identical, though the overall magnitude is somewhat less. To

illustrate this, the $I = 0$ enhancement factor for π -exchange is shown multiplied by a factor of 1.85.

Because the pole of the antibound state in the pp system is closer to threshold than that of the deuteron in np , there is significant energy variation in the ratio of the ($I=1$)/($I=0$) enhancement factors. Nevertheless, as can be seen in Fig. 3, for $k^2 > 0.2 \text{ fm}^{-2}$ the ratio is roughly constant at 1.85. This deviation from unity is important in the understanding of the $pp \rightarrow pp\eta/pn \rightarrow np\eta$ ratio. The empirical approach used in [10], where the wave function squared is evaluated at a fixed radius of 1 fm, would lead to a ratio with a similar energy dependence to that shown in Fig. 3 but lower in magnitude by an overall factor of 0.8

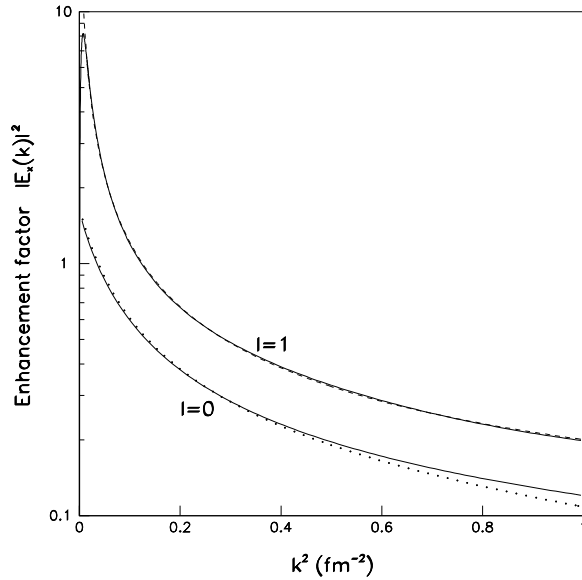


Figure 2: Enhancement factors, defined by Eq. (5.65), evaluated for isospin-one and -zero NN S -waves using Paris wave functions [41]. The solid lines are without the Coulomb repulsion, whereas the broken line includes this effect in the $I = 1$ case. The calculations were done for ρ -exchange but π -exchange leads to a very similar energy dependence though reduced in magnitude by a factor of about 1.85 in the $I = 0$ case and 1.65 for $I = 1$. This is illustrated for $I = 0$ by the dotted curve that has been scaled up by 1.85.

Though the initial-state interaction is expected to vary little with energy, the evaluation of an NN wave function from a potential at energies as high as 1300-1400 MeV is extremely dubious. In order to take the initial flux damping into account, the amplitudes are multiplied by the factor $\eta_L = e^{-Im\{\delta_L\}}$. This is typically 0.77 for the 3P_0 state and 0.73 for 1P_1 .

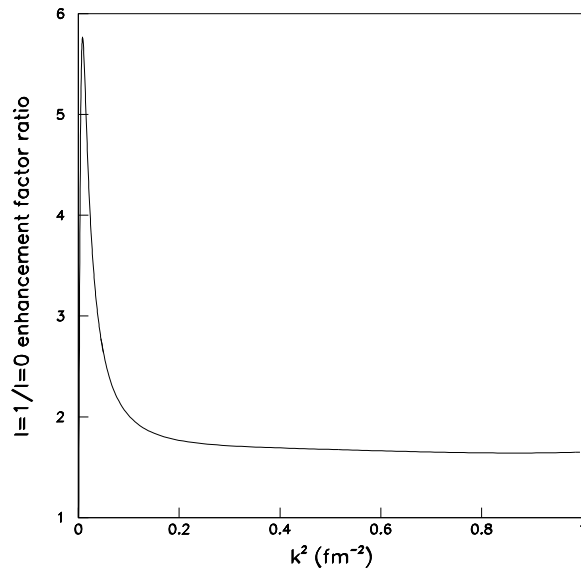


Figure 3: Ratio of enhancement factors for isospin-one and -zero NN final states evaluated for ρ -exchange using Paris wave functions with Coulomb effects [41]. The ratio of the squares of the wave functions at $r \approx 1$ fm is similar in shape but reduced in magnitude by about 20%.

We have neglected the distortion of the final η wave. This is, in part, due to the difficulty of including consistently final state interactions simultaneously in the pp and ηp channels. There is, furthermore, a lack of a realistic η -nucleon potential in the literature. On the basis of potential-model fits to η -nucleon scattering parameters, Garcilazo and Peña predict a strong threshold enhancement in η -deuteron elastic scattering [43]. However, probably as an artefact of their one-term separable assumption, their potentials are extremely attractive at short

distances ($r < 0.2$ fm). Since η -production is sensitive to wave functions at small r , using these potentials as a basis for estimating final state interaction effects can lead to very unrealistic values. We have therefore represented the η by a plane wave though, as we shall see later, there are indications from the production data that this is inadequate.

6 Amplitude for $pn \rightarrow d\eta$

The triangle diagrams describing the $pn \rightarrow d\eta$ reaction are shown in Fig. 4. They are very similar to those for $pn \rightarrow np\eta$ with the addition of a neutron-proton final-state interaction to produce the deuteron.

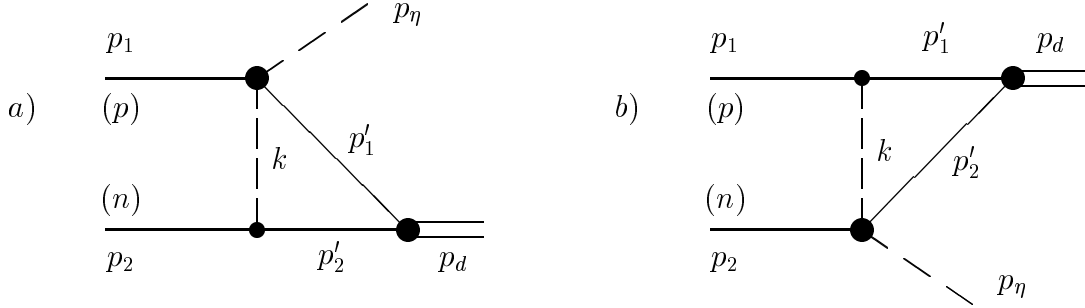


Figure 4: Meson exchange diagrams for $pn \rightarrow d\eta$.

The Feynman amplitude corresponding to Fig. 4a for ρ exchange is

$$\begin{aligned} \mathcal{M}_\rho &= \frac{3}{\sqrt{2}} \int \frac{d^4k}{(2\pi)^4} \frac{-i}{k^2 - m_\rho^2} \bar{u}_c(p_2) \mathcal{M}_\mu(n_c \rightarrow \rho^0 n_c) \\ &\times iS_F^c(p'_2) (-i\Gamma \cdot \epsilon_d^*) iS_F(p'_1) \mathcal{M}^\mu(\rho^0 p \rightarrow \eta p) u(p_1), \end{aligned} \quad (6.66)$$

where we have treated the incident neutron in the charge conjugate representation. Here k is the four-momentum of the ρ -meson and we can neglect the term proportional to $k_\mu k_\nu$ in the ρ propagator since this gives only binding energy contributions. The isospin factor of $3/\sqrt{2}$ takes into account the contribution of charged intermediate mesons. There is, in addition, the diagram of Fig. 4b where the η production takes place at the neutron vertex.

We calculate the triangle diagram in the spectator approximation by performing the integration over q^0 , after suitably closing the contour of integration. This means exploiting formula of Eq. (3.34). After some straightforward manipulations we get in configuration space, as the sum of both ρ -exchange diagrams,

$$\mathcal{M}_\rho = -\frac{3}{\sqrt{2}} (\mathcal{A}_\rho + 2\mathcal{B}_\rho) \mathbf{p} \cdot \boldsymbol{\epsilon}_d^\dagger \eta_i \frac{\sqrt{2M_d}}{2M}$$

$$\times C_\rho \int_0^\infty [\psi_S(r) + 2\psi_D(r)] \bar{Y}_1(m_\rho^*, r) j_0(\frac{1}{2}p_\eta r) \psi_p^{(+)}(r) r^2 dr. \quad (6.67)$$

where $\bar{Y}_1(m_\rho^*, r)$ and C_ρ are defined in Eqs. (5.63) and (5.61).

In a similar fashion, we find the pion-exchange amplitude to be

$$\begin{aligned} \mathcal{M}_\pi &= -\frac{3}{\sqrt{2}} \mathcal{D}_\pi \mathbf{p} \cdot \boldsymbol{\epsilon}_d^\dagger \eta_i \frac{\sqrt{2M_d}}{2M} \\ &\times C_\pi \int_0^\infty [\psi_S(r) + 2\psi_D(r)] \bar{Y}_1(m_\pi^*, r) j_0(\frac{1}{2}p_\eta r) \psi_p^{(+)}(r) \end{aligned} \quad (6.68)$$

with $\bar{Y}_1(m_\pi^*, r)$ and C_π being defined as in Eqs. (5.63) and (5.61), but with m_ρ replaced by m_π .

The contributions from ω and η exchange can be derived immediately from Eqs. (6.67) and (6.68) in an analogous manner to that for $pp \rightarrow pp\eta$.

The η -production operator, especially that part corresponding to ρ exchange, is of short range. At short distances and low energies the deuteron S -state wave function and the $I = 0$ scattering wave functions at low energies are related by the extrapolation theorem [18].

$$\psi_k^{(+)}(r) \approx -\frac{1}{\sqrt{2\alpha(k^2 + \alpha^2)}} \psi_S(r) e^{i\delta_s}, \quad (6.69)$$

where δ_s is the S -wave triplet phase shift. If we neglect the S - D coupling, the relation becomes exact as $k^2 \rightarrow -\alpha^2 = -M \varepsilon_d$, where ε_d is the deuteron binding energy.

By comparing Eq. (6.68) with Eq. (5.61), corrected for isospin and form factor effects, the extrapolation theorem allows us to estimate the triplet contribution to the $pn \rightarrow pn\eta$ cross section in terms of that for $pn \rightarrow d\eta$ independent of the details of the meson exchanges responsible. Generalising the result of Ref. [40], if we parameterise the low energy deuteron cross section estimates as

$$\sigma_{pn \rightarrow d\eta}(Q) \approx a\sqrt{Q} (1 + bQ), \quad (6.70)$$

then the integration over phase space leads to the prediction that

$$\sigma_{pn \rightarrow pn\eta}^{I=0}(Q) \approx \frac{1}{4} x^{3/2} \sqrt{Q} (1 + \sqrt{1+x})^{-2} a \left[1 + \frac{b}{2} Q \left(1 + \frac{1}{2} \frac{x}{(1 + \sqrt{1+x})^2} \right) \right], \quad (6.71)$$

where $x = Q/\varepsilon_d$.

Deviations from the predictions of Eq. (6.70) in our results will mainly arise from corrections to the approximation of Eq. (6.69) in the scattering domain and, in particular, from D -state effects.

7 Results

Since the value of the η -nucleon coupling constant is very poorly known, we shall start by neglecting η exchange, to discuss it later. One would expect, on the basis of Eqs. (4.55) and (4.56), that with pure ρ or π exchange the $pn:pp$ cross section ratio would be a factor of 5, which is not far from the observed value of 6.5 ± 1.0 [5]. This agreement is, however, destroyed by the final-state interaction, which gives a bigger enhancement for the $I = 1$ state than for the $I = 0$ (see Fig. 2). Pure ρ or π exchange would then predict a ratio of 3 or even less.

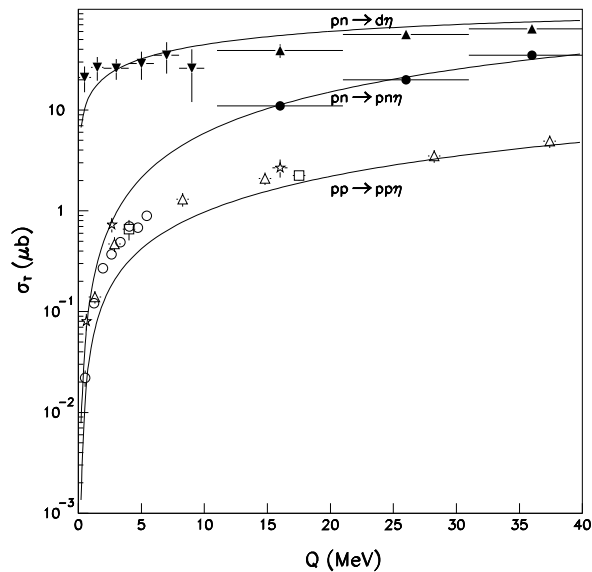


Figure 5: Variation of the total cross sections for the $pp \rightarrow pp\eta$, $pn \rightarrow pn\eta$, and $pn \rightarrow d\eta$ reactions with excess energy. The data are taken from references [1] (square), [2] (open triangle), [3] (star), [4] (open circle), [5] (closed circle), [7] (closed triangle), and [8] (inverted triangle). The curves are the model predictions with standard parameters, evaluated without η exchange.

It was suggested several years ago [11] that the cross section ratio could be increased by invoking a destructive interference between ρ and π exchange in the $I = 1$ channel, and hence constructive in the $I = 0$. With the values of the

parameters given in Section 4, we find the ρ -amplitude to be about three times stronger than that of the π , with the ω term being another factor of three smaller. These values then lead to the broad overall agreement with the $pp \rightarrow pp\eta$ and $pn \rightarrow pn\eta$ total cross sections shown in Fig. 5. The $pn:pp$ ratio is a little too large but, if the ρ coupling were increased by a mere 5%, then this would be reduced to the experimental factor of around 6.5 [5].

Whereas the absolute values of the cross sections and the $pn:pp$ ratio depend very sensitively upon the parameters, the same is not true for the shape of the energy dependence of the $pp \rightarrow pp\eta$ total cross section where the near-threshold values need to be enhanced. The η -nucleon final state interaction, that we have neglected in our analysis, could well supply such an enhancement. The incorporation of such an effect is important but not straightforward and we have made no attempts in this direction.

The largest cross section shown in Fig. 5 near threshold is that for $pn \rightarrow d\eta$, but its dominance is mainly a reflection of the faster rise of the two-body phase space as compared to those of the three-body $pp\eta$ and $pn\eta$ final states. To see this effect in greater detail, we show in Fig. 6 the ratio of the $pn \rightarrow pn\eta$ to the $pn \rightarrow d\eta$ total cross section on a linear scale, where the effect of the rapid phase-space variation can be clearly seen. The theoretical prediction of Eq. (6.71), based upon the extrapolation theorem [18], overestimates the ratio and this would be made slightly worse if the small $I = 1$ contribution were also included. The situation is changed in the full calculation and this is mainly due to the deuteron D -state which increases the $np \rightarrow d\eta$ estimate by up to a factor of two. This large effect is due to the deuteron wave function occurring linearly in Eq. (6.68).

Any residual discrepancies in Fig. 6 may be partially experimental in origin since the data were obtained using a deuterium target and the values of Q deduced by kinematic fitting [5, 6, 7]. The uncertainties in the $pn\eta$ final state are particularly large and one cannot rule out a systematic shift of a few MeV. In order to get better resolution in Q , it would be an advantage to measure the

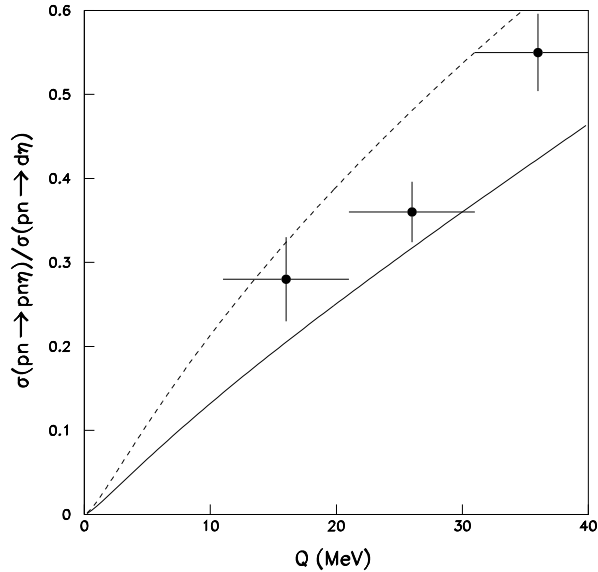


Figure 6: Ratio of the $pn \rightarrow pn\eta$ and $pn \rightarrow d\eta$ total cross sections at the same excess Q . Data from Ref. [5, 6, 7] are compared to the full calculation (solid curve) and the simplified final-state-interaction approach of Eq. (6.71) (broken curve) which only includes $I = 0$ contributions.

spectator proton directly. Such a procedure is now feasible [44].

The results shown in Fig. 5 have been obtained after neglecting η exchange. Now, because of the large ηN elastic amplitude, pure η exchange with an ηNN coupling of $G_\eta^2/4\pi = 1$ would lead to a $pp \rightarrow pp\eta$ cross section twice as big as that for π exchange. If the other parameters were not altered, a value of $G_\eta^2/4\pi = 0.25$ would reduce the $pn:pp$ ratio prediction to below 5. To reproduce this experimental charge ratio with $G_\eta^2/4\pi = 1$, the ρ -exchange amplitude would have to be reduced by a factor of two, and vector meson dominance normally leads to estimates that are far more reliable than that. Since the charge ratio is only weakly affected by initial distortion or choice of NN wave functions or form factor parameters *etc.*, our model indicates that $G_\eta^2/4\pi < 1$ and is probably much smaller.

The $pp \rightarrow pp\eta$ cross section is a function of $\cos^2 \theta_\eta$ because the two initial

protons are identical. From Eq. (3.15) and (4.36), it is seen that to first order in the d -wave amplitudes the differential cross section should be linear in $\cos^2 \theta_\eta$. This is illustrated in Fig. 7, where the predictions, without η exchange, have been increased by 25% before comparing them with the results of [10].

The agreement with experiment is reasonable, except for the largest angle point. The large slope parameter quoted in [10] is due to the weight of this point in the free fit to the data and we see no way whereby such a value could be achieved within the current approach. It should also be noted that this point affects the overall scale, because the angular distribution is normalised to the integrated cross section found in previous studies [2].

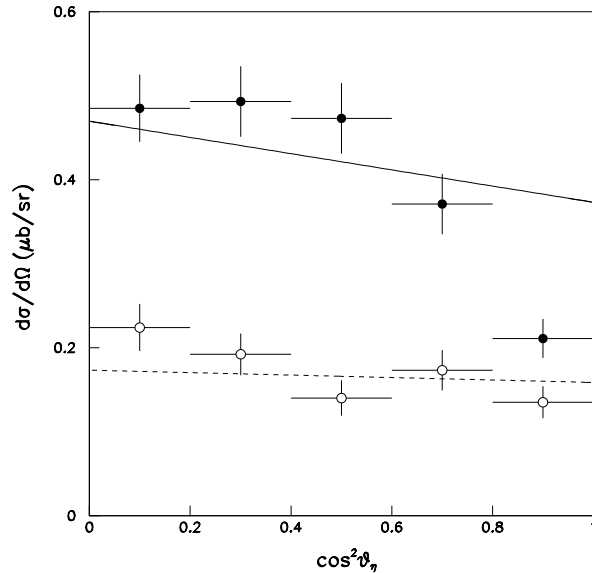


Figure 7: Distribution in the c.m. angle of the η in the $pp \rightarrow pp\eta$ reaction at $Q = 37$ MeV (closed circles) and $Q = 16$ MeV (open circles) from [10]. The predictions of our model with standard parameters without η exchange, shown as the corresponding solid and broken lines respectively, have been increased by a factor of 1.25.

Though small, the slope is still much larger than that found for $\gamma p \rightarrow \eta p$ [32]

or $\pi^- p \rightarrow \eta n$ [29]. It is here important to note that the photoproduction data are maximal for $\theta_\eta \approx 90^\circ$ where the pion-production results show a minimum. To get agreement with the pn/pp total cross section ratio, the ρ and π contributions must cancel in the pp case, and this enhances the curvature and leads to the agreement shown in Fig. 7. For $pn \rightarrow pn\eta/d\eta$ the interference is constructive and we would expect the slope to be an order of magnitude smaller.

There are, as yet, no data on the analysing power A_y in $pp \rightarrow pp\eta$, though there is an approved proposal at COSY-11 to attempt the first investigation [45]. There are also no measurements of A_y in $\pi^- p \rightarrow \eta n$ but, if we consider only ρ exchange, we predict that A_y for $pp \rightarrow pp\eta$ should be of the same size as that for $\gamma p \rightarrow \eta p$ [37] at the same value of the η - N momentum. With the parameterisation of Eqs. (3.29, 3.30), one expects that the analysing power to vary as

$$A_y = 2 A_y^{\max} \sin \theta_\eta \cos \theta_\eta. \quad (7.72)$$

The predicted energy dependence of the maximum value of the analysing power A_y^{\max} is shown in Fig. 8. The values are small because of the node in the input of Eq. (3.30) at $\eta \approx 0.4$, and so they may be sensitive to the neglected p -wave and pion-exchange terms. It may be of interest to note, however, that the maximum occurs for $Q \approx 10$ MeV, which is a region where the acceptance of the COSY-11 spectrometer is significant [45].

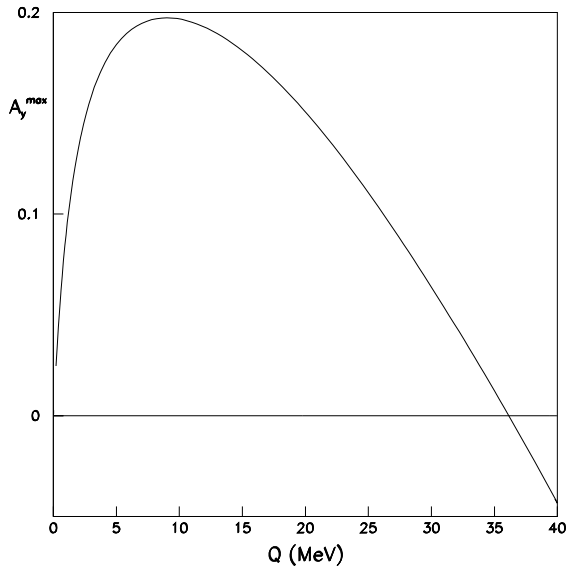


Figure 8: Predicted value of the $pp \rightarrow pp\eta$ maximum analysing power coefficient of Eq. (7.72) as a function of excess energy, estimated assuming only vector-meson exchange.

8 Conclusions

We have been able to describe, within a one-meson-exchange picture, the main features of the experimental data on η production in nucleon-nucleon collisions near threshold. Although most of the energy dependence is reproduced, this is mainly an effect of phase space, combined with the nucleon-nucleon final-state interaction. The remaining low- Q deviations in both the $NN \rightarrow NN\eta$ and $pn \rightarrow d\eta$ reactions could be due to the η -nucleon final-state interaction that was not included in the calculation.

The good agreement with the magnitude of the $pp \rightarrow pp\eta$ total cross section may, in part, be fortuitous given the uncertainties in the the coupling constants and other parameters, including those arising from the use of vector-meson dominance to extract the input amplitudes. Although we have not adjusted the input in order to fit the data, it should be stressed that there remains significant flexi-

bility in the numerical predictions arising from these uncertainties.

A more serious worry is the sensitivity to the short-range variation of the nucleon-nucleon wave functions arising from the form of the production operators. The Paris NN potential [41], that we have used in all our estimates, is essentially local and this has a significant repulsive core that suppresses the wave functions at short distances. On the other hand, the Bonn potential [24, 21] has a non-local component that allows the core to be much softer and this results in much less small- r suppression. This means that the evaluation of the $pn \rightarrow d\eta$ cross section on the basis of the integrals in Eqs. (6.67, 6.68) is about three times bigger for the Bonn deuteron wave function than that of Paris. The difference would be even larger without form factors to regularise the production operators at short distances. We would argue that, because we are using local production operators, then it is more logical to use wave functions corresponding to a local potential. The $np \rightarrow d\eta$ cross section is sensitive to the deuteron D -state wave function at short distances and the ratio of this to the S -state also differs significantly between Paris and Bonn.

In our approach, the ρ -exchange amplitude is bigger than that of the π and it is particularly reassuring that the destructive interference required to give good agreement for the ratio of the $pn \rightarrow pn\eta/pp \rightarrow pn\eta$ cross sections is such as to give the correct shape of angular dependence in the $pp \rightarrow pp\eta$ case. It should be noted that if the π -exchange term were to dominate, then the slope of the differential would have the sign opposite to that of experiment. This illustrates the importance of analysing all the η -production channels simultaneously.

The uncertainty in the ηNN coupling constant makes it impossible to estimate the η -exchange term with any reliability. It cannot be too large without destroying the good agreement with the pn/pp ratio and this allows us to derive the upper limit *within the model* of $G_{\eta NN}^2/4\pi < 1$. It should be noted in this context that the η contribution in semi-phenomenological nucleon-nucleon potentials [24, 41] is to be associated with the exchange quantum numbers and not necessarily purely with the true η -meson.

Although our predictions for the slope in $pp \rightarrow pp\eta$ are compatible with the data, it must be admitted that the experimental measurements are still far from definitive in both statistical and systematic aspects. A significant improvement is to be expected in the results through the use of the WASA detector [46]. This is designed for the study of rare decays of the η but the production of the meson will also be investigated as a by-product under very good conditions. One test of our model is the prediction that the η angular distributions in the proton-neutron cases should be much flatter than for proton-proton. This could be checked in the $pn \rightarrow d\eta$ reaction, where the measurement of all fast final-state particles means that the kinematics may be well defined even without detecting the spectator proton [46]. The only measurements extant showed an η distribution that was consistent with isotropy [6].

Another partial check on our model could come from a measurement of the beam analysing power in $pp \rightarrow pp\eta$. This is predicted to have a maximum, albeit rather small, at quite low values of Q . The predictions are not conclusive because of the lack of $\pi^-p \rightarrow \eta n$ analysing power input to complement the extensive unpolarised differential cross section data which should appear in the near future [26].

The gravest drawback in the calculation is the neglect of η rescattering. There are as yet no well-behaved η -nucleon potentials in the literature and the short range of the η -production operator means that this effect will depend upon the details of the η -nucleon interaction and not just the on-shell t -matrix. A consistent three-body treatment of the ηNN final state in η production is a challenge still to be met.

We are grateful to members of experimental groups at Saclay, CELSIUS, and COSY for discussions about η production over many years. The present work has been helped by correspondence with T. Peña and L. Tiator. S. Prakhov and B.M.K. Nefkens provided us with valuable information on the Crystal Ball programme. This work has been supported by the Royal Swedish Academy of

Sciences, within the framework of the European Science Exchange Programme. One of the authors (CW) would like to thank the The Svedberg Laboratory for its generous hospitality. We would like to dedicate the paper to our friend Nimai Mukhopadhyay with whom we shared a common interest in η -production over many years.

References

- [1] Chiavassa, E. *et al.*, Phys. Lett. B **337**, 192 (1994).
- [2] Calén, H. *et al.*, Phys. Lett. B **366**, 39 (1996).
- [3] Hibou, F. *et al.*, Phys. Lett. B **438**, 41 (1998).
- [4] Smyrski, J. *et al.*, Phys. Lett B **474**, 182 (2000).
- [5] Calén, H. *et al.*, Phys. Rev. C **58**, 2667 (1998).
- [6] Häggström, S., PhD thesis, Uppsala University, Acta Universitatis Upsaliensis **13** (1997).
- [7] Calén, H. *et al.*, Phys. Rev. Lett. **79**, 2642 (1997).
- [8] Calén, H. *et al.*, Phys. Rev. Lett. **80**, 2069 (1998).
- [9] Plouin, F., Fleury, P. and Wilkin, C., Phys. Rev. Lett. **65**, 690 (1990).
- [10] Calén, H. *et al.*, Phys. Lett. B **458**, 190 (1999).
- [11] Germond, J.-F. and Wilkin, C., J. Phys. G **15**, 437 (1989); Nucl. Phys. A **518**, 308 (1990).
- [12] Laget, J.M., Wellers, F., and Lecolley, J.F., Phys. Lett. B **257**, 254 (1991).
- [13] Vetter, T., Engel, A., Biró, T. and Mosel, U., Phys. Lett. B **263**, 153 (1991).
- [14] Moalem, A., Gedalin, E., Razdolskaya, L. and Shorer, Z., Nucl. Phys. A **600**, 445 (1996).
- [15] Batinić, M., Švarc, A. and Lee, T.-S.H., Physica Scripta **56**, 321 (1997).
- [16] Peña, M.T., Garcilazo, H. and Riska, D.O., Nucl. Phys. A **683**, 322 (2001).
- [17] Grishina, V.Yu. *et al.*, Phys. Lett. B **475**, 9 (2000).
- [18] Fäldt, G. and Wilkin, C., Nucl. Phys. A **604**, 441 (1996).

- [19] Mayer, B. *et al.*, Phys. Rev. C **3**, 2068 (1996).
- [20] Willis, N. *et al.*, Phys. Lett. B **406**, 14 (1997).
- [21] Machleidt, R., Phys. Rev. C **63**, 024001 (2001).
- [22] Zhu, S.-L., Phys. Rev. C **61**, 065205 (2000).
- [23] Tiator, L., Bennhold, C. and Kamalov, S.S., in “Physics with GeV-Particle Beams” (Eds. H. Machner. and K. Sistemich) (World Scientific, Singapore, 1995).
- [24] Machleidt, R., Holinde, K. and Elster, Ch., Phys. Rep. **149**, 1 (1987).
- [25] Benmerrouche, M., Mukhopadhyay, N.C. and Zhang, J.F., Phys. Rev. D **51**, 3237 (1995).
- [26] Sadler, M.E., πN Newsletter, **13**, 123 (1997).
- [27] Binnie, D.M. *et al.*, Phys. Rev. D **8**, 2789 (1973).
- [28] Kozlenko, N.G., Acta Phys. Polon. B **31**, 2239 (2000).
- [29] Prakhov, S. and Nefkens, B.M.K., private communication (2000).
- [30] Batinić, M., Dadić, I., Šlaus, I., Švarc, A., Nefkens, B.M.K. and Lee, T.-S.H., Physica Scripta **58**, 15 (1998).
- [31] Green, A.M. and Wycech, S., Phys. Rev. C **60**, 035208 (1999).
- [32] Krusche, B. *et al.*, Phys. Rev. Lett. **74**, 3736 (1995); Phys. Lett. B **397**, 171 (1997); Krusche, B., Habilitationsschrift, Gießen, 1995.
- [33] Sakurai, J.J., Phys. Rev. Lett. **17**, 1021 (1966).
- [34] Benayoun, M. *et al.*, Eur. Phys. J. C **2**, 269 (1998).

- [35] Bauer, T.H. *et al.*, Rev. Mod. Phys. **50**, 261 (1978); Leith, D.W.G.S., in “Electromagnetic Interactions of Hadrons”, Vol. 1 (Eds. A. Donnachie and G. Shaw) (Plenum Press, New York, 1978).
- [36] Tiator, L., Dreschel, D., Knöchlein, G. and Bennhold, C., Phys. Rev. C **60**, 035210 (1999).
- [37] Bock, A. *et al.*, Phys. Rev. Lett. **81**, 534 (1998).
- [38] Thompson, R. *et al.*, Phys. Rev. Lett. **86**, 1702 (2001).
- [39] Goldberger, M.L. and Watson, K.M., “Collision Theory” (John Wiley, N.Y., 1964).
- [40] Fäldt, G. and Wilkin, C., Physica Scripta **56**, 566 (1997).
- [41] Lacombe, M. *et al.*, Phys. Rev. C **21**, 861 (1980); Lacombe, M. *et al.*, Phys. Lett. B **101**, 139 (1981); Loiseau, B., private communication.
- [42] Arndt, R.A. *et al.*, <http://gwdac.phys.gwu.edu/>
- [43] Garcilazo, H. and Peña, M.T., Phys. Rev. C **61**, 064010 (2000).
- [44] Bilger, R. *et al.*, Nucl. Instr. Meth. **457**, 64 (2001).
- [45] Oelert, W. *et al.*, COSY-11 proposal 77.1 (1999) (unpublished).
- [46] Kullander, S., “Proc. 14th Int. Conf. on Particles and Nuclei”, (World Scientific, Singapore, 1997), p. 754.